

## Exploring the causes of an extreme flood event in Central New York, USA

Peng Gao & Justin J. Hartnett

To cite this article: Peng Gao & Justin J. Hartnett (2016): Exploring the causes of an extreme flood event in Central New York, USA, Physical Geography, DOI: [10.1080/02723646.2016.1153332](https://doi.org/10.1080/02723646.2016.1153332)

To link to this article: <http://dx.doi.org/10.1080/02723646.2016.1153332>



Published online: 26 Feb 2016.



Submit your article to this journal [↗](#)



View related articles [↗](#)



View Crossmark data [↗](#)

## Exploring the causes of an extreme flood event in Central New York, USA

Peng Gao and Justin J. Hartnett

Department of Geography, Syracuse University, Syracuse, NY, USA

### ABSTRACT

This study examined the causes of an extreme flood event on 28 June 2013 in Central New York, USA by comparing its hydrological, hydrometeorological, and rainfall-runoff transformation characteristics with those of a typical flood event. Flood frequency analyses showed that the maximum rainfall intensity and the peak discharge of the extreme event had recurrence intervals (RIs) of 8 and 86 years, respectively, while RIs for the typical event were 42 and 11 years, respectively. Their severity diagrams and quantification of their rainfall spatial variations illustrated that the extreme event was spatially localized with high intensities, whereas the typical event was spatially uniform and prolonged. Watershed modeling indicated that the rainfall-runoff transformation was dominated by the infiltration excess process for the extreme flood, while controlled by both infiltration and saturation excess processes for the typical event. These analyses revealed that the upgrade-magnitude conversion pattern of the extreme flood event was induced by the spatial pattern of the rainfall and the "lubricant" effect of the watershed, and emphasized the need for better understanding of such type of extreme events.

### ARTICLE HISTORY

Received 20 September 2015  
Accepted 9 February 2016

### KEYWORDS

Extreme flood event; rainfall intensity; severity diagram; rainfall-runoff processes

## Introduction

Flooding is one of the major natural disasters, often causing severe damage in modern societies (Arghius, Ozunu, Samara, & Rosian, 2014; Cross, 2014; Death, Fuller, & Macklin, 2015; Marchi et al., 2009). Increased flooding incidents have been observed world-wide in recent decades (Billi, Alemu, & Ciampalini, 2015; Huntington, 2006; Kundzewicz et al., 2013; Mallakpour & Villarini, 2015). One well-known cause is anthropogenic activities. Intensified agricultural practices in watershed uplands and expansion of cities and towns have increased hillslope soil erosion and in-channel sediment deposition, leading to channel bed accretion and the reduction of channel storage capacity (CNYRPDB, 2003; He, Zhou, Yu, Tian, & Chen, 2007; Yin & Li, 2001). These activities have increased the frequency of floods by reducing the magnitude of peak discharges that may cause flooding. For example, the frequency of floods in the middle reach of the Yangtze River has increased since 1950,

yet their recurrence intervals (RIs) have reduced from greater than 16.5 years to just over 2.5 years (Yu, Chen, Ren, & Yang, 2009).

In addition to physically changing the landscape, increasing evidence suggests that climate change alters patterns in extreme weather, including heavy rainfall events (Kundzewicz et al., 2013; Matthews, Murphy, Wilby, & Harrigan, 2014; Méndez-Lázaro, Nieves-Santiago, & Miranda-Bermúdez, 2014; Mendizabal, Sepúlveda, & Torp, 2014; Schiermeier, 2011; Stevenson & Schumacher, 2014). As a result, the likelihood of extreme floods increases (Foulds, Griffiths, Macklin, & Brewer, 2014; Jena, Chatterjee, Pradhan, & Mishra, 2014; Zhang et al., 2013), a change that has become more prevalent in recent decades. If global average temperatures continue to increase (IPCC, 2013), more incidents of extreme weather could emerge, possibly leading to more extreme floods in the future (Apurv, Mehrotra, Sharma, Goyal, & Dutta, 2015).

However, neither anthropogenic activities nor climate change may directly explain the reasons behind the extreme flood event that occurred in the Oneida Creek Watershed of Central New York on 28 June 2013. Although the rainstorm was relatively intense, the degree of intensity was not unusually high and the storm only lasted for about 12 h. Both its magnitude and duration were apparently not extreme. Yet, induced by what appeared as a rather innocuous rainstorm, this flood was severe enough to prompt Governor Andrew Cuomo of the State of New York to issue a Disaster Declaration for the region. Situated within the Oneida Creek Watershed, the City of Oneida, population of about 11,400, is located in eastern Central New York. Its population, economic conditions, and upstream land use/cover types have not significantly changed over recent years, suggesting that the severe damage induced by the flood was not directly caused by local anthropogenic activities.

Then, why could a frequent storm cause an extreme flood event? A plausible explanation may be drawn from the established fact that the spatial variability of a rainstorm can cause an extreme flood event (Arnauda, Bouvier, Cisneros, & Dominguez, 2002; Faures, Goodrich, Woolhiser, & Sorooshian, 1995; Schuurmans & Bierkens, 2007). In particular, the geographic distribution of rainfall intensities (Saulnier & Le Lay, 2009) might account for the occurrence of an extreme flood even with a relatively small storm event. Nonetheless, the precipitation of a storm must go through the complex rainfall-runoff processes before turning into stream flows of a watershed. An important, but often ignored feature of these processes is the filtering role of a watershed – that is, the spatially heterogeneous change of precipitation may be smoothed, the degree of which depends on the physiographic conditions of the watershed (Andres-Domenech, Garcia-Bartual, Montanari, & Marco, 2015). The most likely consequence might be that the magnitude of the peak discharge with regard to the RI tends to be less than that of the precipitation for a given event (Billi et al., 2015; Fuller, 2007), which is contradictory to the above-mentioned event.

The purpose of this study is to understand the causes of this extreme event by exploring both spatial and temporal distribution of rainfall, and the associated hydrological response. Various statistical methods (e.g. time series and geostatistical analyses, and statistical modeling) have been used to explore spatial and temporal variations of rainfall time (from daily to annual) series, or within a single rainfall event (Bargaoui & Bardossy, 2015; Carvalho & Woodroffe, 2015; Gamoyo, Reason, & Obura, 2015; Han et al., 2015; Panthi et al., 2015). Methods such as numerical weather prediction models, spatial interpolations, and stochastic rainfall generators have also been commonly used to investigate how the predicted spatial distribution of rainfall affects the stream flow predicted by a hydrological model (Borga,

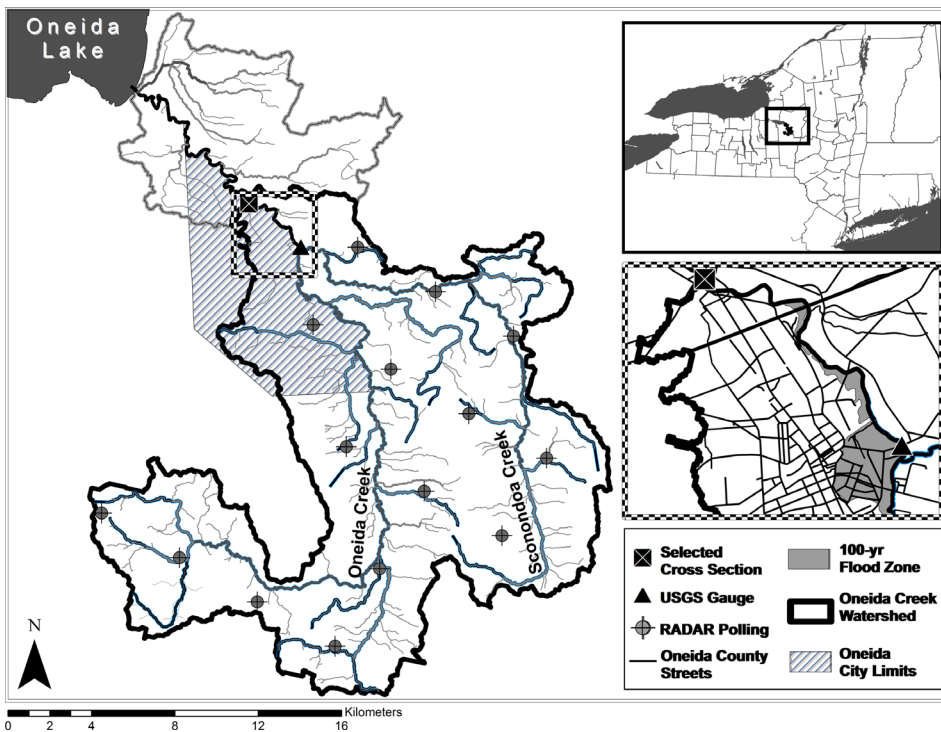


**Figure 1.** Locations of the study watershed, Oneida City, USGS gaging station, measured cross section, flood zone of the extreme event, and 15 radar stations.

Anagnostou, Bloschl, & Creutin, 2011; Guo, Wang, Zeng, Ma, & Yang, 2015; Mirus, Ebel, Heppner, & Loague, 2011; Vincendon, Ducrocq, Nuissier, & Vié, 2011). Our study was different from these in that it examined how different spatial and temporal distributions of storm events may lead to different hydrological responses and the consequential variations in the magnitude (in terms of the RI) of both storm events and the resultant peak discharges. The study provided an additional perspective of understanding the causality between rainfall and the resultant flood event.

For this purpose, we selected another representative event to compare its magnitudes of rainfall and peak flow against those of the extreme event. First, we examined the hydrological features and the associated geomorphological response of the selected two events. Second, we analyzed magnitudes, intensities, and spatial variabilities of the two associated rainfall events. Third, we quantified the degrees of spatial variability of the two events within the study watershed. Finally, we simulated the rainfall-runoff processes of these two events using an event-based hydrological model to reveal the cause of the extreme flood.

## Materials and methods

### *Study area and the flood event*

Oneida Creek watershed, covering 387 km<sup>2</sup>, is located in eastern Central New York. Its main stream, Oneida Creek, drains into glacially formed Oneida Lake (Figure 1). The upper part

of the watershed is on a north-facing escarpment with a series of steep hills and valleys that geologically belong to the Appalachian Upland region. The middle and lower parts have low lying, flat lands that are within the Lake Plain (CNYRPDB, 2003). This geological structure controls the morphology of Oneida Creek: the upstream reach is characterized by steep, bedrock channels with waterfalls, while the middle and lower channel reaches are more meandering with gravels and sand covering the beds, and silts and clays forming the banks. The City of Oneida spreads around the west wing of the lower and middle reaches of the Creek (Figure 1). Its center of business and residence is adjacent to Oneida Creek and hence has suffered numerous floods in the past century (ABDCE, 1973). On 28 June 2013, a heavy rainfall resulted in unexpected havoc for the city. About 8 h after the onset of rainfall, flow in the lower reach passing through the city center began to overtop the bank, inundating 0.62 km<sup>2</sup> within the city. The flooding prompted evacuations of approximately 225 dwellings and 25 commercial businesses. Following the flood, approximately 29 of those structures threatened the health, safety, and/or welfare of the occupants or public and thus needed to be demolished. The flood created more than 1600 tons of waste in the inundated area, which was suspected to be similar to that of the 100-year flood zone determined by FEMA (Figure 1). These damages led to more than 1.35 million US dollars of direct economic loss.

To understand the causes of the flood, we examined the channel cross section about 1 km downstream of the USGS gaging station near the confluence of the main stream (Oneida Creek) with its main tributary (Sconondoa Creek) (Figure 1). Geomorphologically, this cross section serves as the outlet for the middle and upstream sub-watershed (termed the study watershed hereafter) with an area of 311 km<sup>2</sup> (Figure 1). Thus, the arriving flows are controlled by physiographic conditions of the study watershed and the precipitation falling within it. Agricultural and urban lands, mixed with forest and pasture lands, dominate the study watershed. Its stream network is well developed with a drainage density of 1.3 (km/km<sup>2</sup>). Therefore, the response time of runoff to rainfall is generally short, leading to a typically steeper rising limb than the associated falling limb of a hydrograph for a given storm event (Gao & Josefson, 2012a).

## Methods

In addition to this event, we selected the one with the second largest peak discharges since 2010 for comparison. The two events, ordered by the magnitude of their peak discharges, are denoted as the 6/28/2013 and 9/8/2011 events. Detailed methods are described as follows.

### *Hydrological and geomorphological analyses*

We performed flood frequency analysis (FFA) to determine RIs of the two peak discharges, using annual peak discharges between 1950 (the earliest available year) and 2010 (the latest year before the selected events) from the existing USGS gaging station (Figure 1). For each event, we compared the goodness-of-fit among three commonly used probability distributions (i.e. log-Pearson type III, extreme value distribution, and normal distributions) (Chow, Maidment, & Mays, 1988) and found that the first distribution best fit the data. We then established the relationship between the discharges predicted using this distribution and the associated plotting positions, which were calculated using the Weibull formula (McCuen, 2004), and determined the RIs of the two peak discharges. We also calculated (1) the total event runoff volume, and (2) the steepness of the rising limb of the hydrograph, defined as

a ratio of the difference between peak discharge and the base flow before the given event to the time lag between these two discharges.

Geomorphologically, we surveyed the selected channel cross section annually from 2009 to 2012. Comparison of these measured profiles indicated that the cross section has not substantially changed since 2009. One month after 28 June 2013, we revisited it and observed no significant morphological changes. Thus, we concluded that this selected cross section has remained relatively stable. On this ground, we created a typical cross-section profile using the survey data collected on 12 September 2011 and calculated the “representative” bankfull discharge using the method elaborated in Gao and Puckett (2012). Moreover, we compared the water levels of the two peak discharges with that of the bankfull discharge at this cross section.

### *Hydrometeorological analyses*

*Point rainfall intensities and areal magnitudes.* We obtained extreme precipitation data from the Cornell Extreme Precipitation web page: <http://precip.eas.cornell.edu/>. The data were classified into rainfall intensities for every 1, 2, 3, 6, 12, and 24 h. Each rainfall intensity included precipitation values with their associated RIs of 1, 2, 5, 10, 25, and 50 years. Using these data, we created a series of curves representing rainfall intensities against time intervals, each of which reflected one of the six RIs. These data represented magnitudes of point rainfall intensities for different time intervals.

The study watershed consists of 15 point locations (hereafter referred to as weather stations) where daily and hourly precipitation data were downloaded from <http://water.weather.gov/precip/download.php> and [http://www.srh.noaa.gov/ridge2/RFC\\_Precip/](http://www.srh.noaa.gov/ridge2/RFC_Precip/), respectively. Daily data were the sum of hourly data for each day, and hourly data were compiled in three steps. First, distributed precipitation data were calculated from the real-time (hourly) radar image. Second, a correction factor was calculated by comparing these calculated data with real precipitation data obtained from ground rainfall gages. Third, quality control was implemented to remove gages that appear to be malfunctioning as well as radar artifacts that may appear. Hourly precipitation data determined in this manner were much more accurate than the original radar data.

Yet, these data still involved uncertainties derived from potential errors in radar data due to problems such as bright banding and radar range degradation, and in gage data due to problems such as gage siting and under measurement during high intensity rainfall events. Although *in situ* measurements of rainfall data were not available to minimize these uncertainties, as Paixao et al. (2015) had done, two reasons allowed us to believe that the downloaded data had sufficient accuracy for this study. First, precipitation data of the same quality for the two selected events were used for comparing their relative magnitudes only. Therefore, the comparison was less affected by the above-mentioned uncertainties. Second, which is more important, the uncertainties in the precipitation data were compensated for during rainfall-runoff modeling by adjusting the parameters of the watershed model, as described later.

Using these data, we calculated rainfall totals for 2, 3, 6, and 12 h at each station, as well as the maximum point precipitation for each time interval. These values were subsequently compared with the curves of extreme precipitation to determine RIs of the associated rainfall intensities. For each event, the mean rainfall total over all 15 stations was calculated for each time interval to represent the rainfall intensity of the associated time interval, and the mean

of the total precipitation in each of the 15 stations was calculated as the total precipitation of the given rainfall event at that station.

**Rainfall severity diagrams.** Point rainfall intensities fail to describe the spatial variability of rainfall, such that storms that have the maximum point intensities of the same RI may lead to flood events of different magnitudes (Simoes et al., 2015). To take it into consideration, we created the severity diagrams of the two selected events, which map the distributed rainfall RIs with the two axes representing rainfall durations and surface areas within a given watershed (Ramos, Creutin, & Leblois, 2005). The severity diagram represents the magnitude of a storm event over a range of spatial and temporal scales within a normalized framework and hence allows for the comparison of storm structures among different events (Vié et al., 2012). Following the general procedure described in Ceresetti, Anquetin, Molinié, Leblois, and Creutin (2011), we first created intensity-duration-frequency (IDF) curves for different RIs using the historical rainfall data. Then, we generated areal reduction factor (ARF) figures and determined the ARF for each areal precipitation value we calculated. At last, we combined IDF with ARF to determine the return period for a given rainfall duration and surface area (Ceresetti et al., 2011). Using these results, we created severity diagrams for the two storm events.

**Quantifying rainfall spatial and temporal variability.** Although the severity diagram illustrates graphically the spatial and temporal patterns of a rainstorm, it is incapable of providing quantitative measures that distinguish the degrees of spatial variability of different rainfall dynamics. To fill the gap, we quantified the spatial and temporal variability of a given rainfall storm as follow. First, we classified the hourly rainfall intensity of a storm over the entire study watershed into three categories separated by 12.7 and 6.35 mm/h. For a storm lasting about 24 h with the intensity of 6.35 mm/h, the total precipitation from the event (i.e. 152.4 mm) would classify this storm as a heavy rainfall event based on the historical rainfall data within the study watershed. Thus, areas with a rainfall intensity greater than 12.7 mm/h, between 12.7 and 6.35 mm/h, and less than 6.35 mm/h had very intensively, intensively, and less intensively localized rainfall, respectively. Second, we calculated the area associated with each rainfall category and the corresponding proportion for 8 consecutive hours. Selection of 8 h enabled us to best distinguish the temporal difference of hourly rainfall between the two selected events. Using these values, we can quantify different degrees of localization between the two.

### **Modeling rainfall-runoff dynamics**

We first calculated the runoff coefficient (Beven, 2001) to determine the overall effectiveness of the rainfall-runoff transformation for the two storm events. Then, we simulated their rainfall-runoff dynamics to reveal the mechanisms leading to their difference using a physically-based watershed model, Dynamic Watershed Simulation Model (DWSM). DWSM relies on a series of mathematic equations to characterize during a storm event various hydrological and in-stream routing processes, as well as sediment transport dynamics (Borah, Bera, & Xia, 2004). Spatially, DWSM divides a watershed into a series of overland elements and the connected stream segments. It predicts hydrograph and sedigraph at the outlet of the watershed for an event, as well as the peak discharge ( $Q_{\text{peak}}$ ), total runoff volumes ( $V$ ) and event sediment yields for all spatially divided elements.

Our study watershed was divided into 42 overland elements and 21 connected channel segments. The details were described in an earlier study (Gao, Borah, & Josefson, 2013). A fundamental input data-set of DWSM is precipitation. For the two selected events, we were able to obtain hourly rainfall data from the 15 weather stations located within the study watershed (Figure 1). Environmental factors such as overland slope, channel length, and vegetation coverage were calculated as single area-weighted values for each element and segment. The modified curve number (CN) method imbedded in DWSM (Borah, Xia, & Bera, 2002) was used to simulate the runoff generation processes. According to this method, there are five adjustable parameters, CN, friction factors ( $f_o$ ), lateral saturated hydraulic conductivity (COND), initial soil moisture content (CONT) for overland elements, and friction factor for channel segments ( $f_c$ ). These values vary among overland elements and channel segments to reflect the spatial heterogeneities of topography, soil types, and land use/cover types (Gao, Borah, & Yi, 2015).

Rainfall excess rate ( $Q_r$ , mm) is commonly determined by Borah (2011):

$$Q_r = \frac{(P - aS_r)^2}{P + (1 - a)S_r} \quad (1)$$

$$S_r = \frac{25,400}{CN} - 254 \quad (2)$$

where  $P$  is the accumulated rainfall (mm) and  $a = 0.2$  is the initial abstraction factor, which is a fraction of the potential maximum retention and thus dimensionless (Bedient & Huber, 2002; Gonzalez, Temimi, & Khanbilvardi, 2015). However, many studies have shown that the coefficient,  $a$  may be as low as 0.05 and vary from place to place (Hawkins, Ward, Woodward, & Van Mullem, 2008; Soulis & Valiantzas, 2012). So, we allowed it to be variable and treated it as the sixth adjustable parameter in our modeling.

During simulation, CN values were varied through CNAF, whose change affected at the same rate the values of CN for all overland elements and hence accounted for variations in the antecedent soil moisture (ASM) conditions, as well as estimation errors in precipitation and CN (Gao et al., 2015). The parameter  $a$  remained the same for all overland elements. Its variation indirectly affects CN values and directly accounts for interception loss and depression storage (McCuen, 2004), which affects the “ponding time” of the rainfall falling on a surface and hence the time when surface runoff emerges. FAFO and FAFC are parameters, whose changes affected at the same rate the values of  $f_o$  and  $f_c$ . Their changes reflected variations of Manning’s  $n$  from storm to storm for overland elements and channel segments. Values of COND and CONT are relevant to the magnitude of the event subsurface flow. For a given storm, CNAF has the highest impact on the predicted hydrograph, while FAFO and FAFC mainly influence the arriving time of the peak discharge ( $Q_{\text{peak}}$ ) (Gao et al., 2015).

For the two selected events, we generated the best-fitted hydrograph based on the goodness-of-fit assessment represented by the percent errors of  $Q_{\text{peak}}$  and its arrival time, and total runoff volume ( $V$ ) between predicted and measured ones. Comparing the difference of these six parameters allowed us to identify different hydrological responses of the study watershed to the two events. We also used DWSM to predict values of  $Q_{\text{peak}}$  in each overland

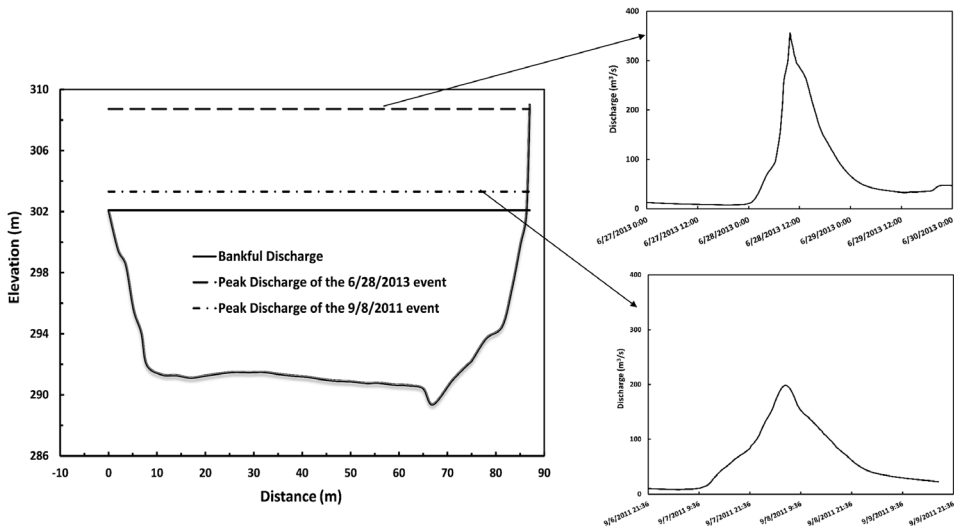


**Figure 2.** Profile of the representative cross section at the outlet of the study watershed with positions of peak discharges and hydrographs for the two selected hydrological events.

element for the two events and compared these values to show the different spatial patterns of runoff between the two events.

## Results and analyses

### *Hydrological characteristics of the two events*

The two selected events (6/28/2013 and 9/8/2011) had peak discharges of 355 and 199 m<sup>3</sup>/s, respectively, and their total runoff volumes were 1.33 and 1.14 × 10<sup>7</sup> m<sup>3</sup>, respectively. These values evidently showed that the 6/28/2013 event had a much higher magnitude of the two. In addition, the slope of the rising limb of the event hydrograph was 6.44 and 1.76 × 10<sup>3</sup> m<sup>3</sup>/h<sup>2</sup>, respectively, indicating the 6/28/2013 event had a much faster flow response to rainfall (Figure 2).

The summer event (on 6/28/2013) created a peak discharge much greater than the representative bankful discharge ( $Q_{bf}$ ), which is about 150 m<sup>3</sup>/s (Gao & Josefson, 2012b). During the event, about 50% of the flow in volume overflowed the bank at the selected cross section. Although the peak discharge of the fall event (on 9/8/2011) was higher than  $Q_{bf}$ , it merely resulted in limited overflow with inundation in the lower adjacent area around the cross section (Figure 2).

FFA showed that RI of the two events was 86, and 11 years, respectively, while that for  $Q_{bf}$  was about 5 years. The peak discharge of the 6/28/2013 event was indeed larger than any recorded annual maximum peak discharge since the beginning of the gage records in 1950. Although we did not measure the extent of the flooded area, it was close to the boundary of the 100-year flood zone (Figure 1) according to observations from local residents and agencies. The inundated area was also comparable to that flooded by an extreme event in June, 1922 (ABDCE, 1973). Obviously, the 6/28/2013 event was a historical flood whose magnitude was much greater than that of the 9/8/2011 event.

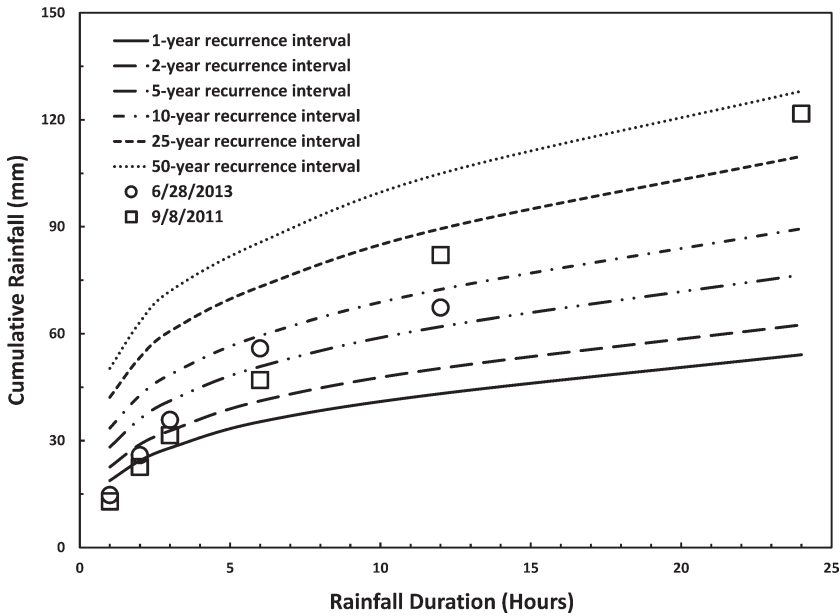


**Figure 3.** The maximum point rainfall intensities at 1-, 2-, 3-, 6-, 12-, and 24-h for the two selected storm events. Note: The curves represent regional RIs for comparison.

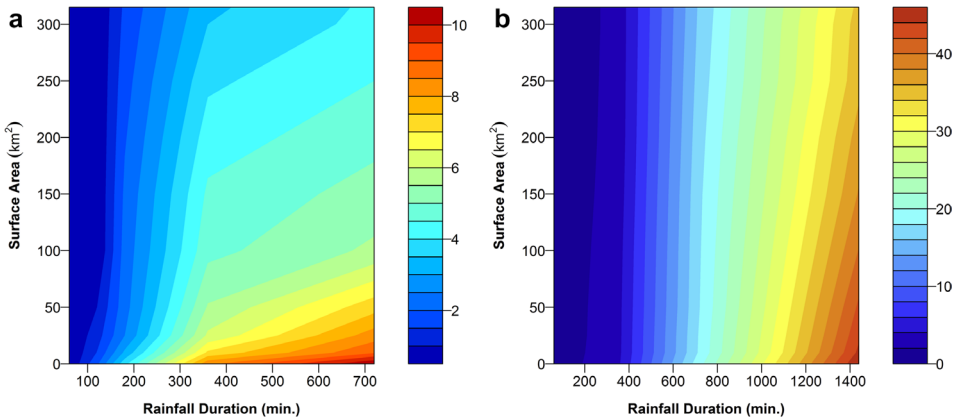


**Figure 4.** Severity diagrams of the two selected events. (a) The 6/28/2013 event and (b) the 9/8/2011 event. Note: The range of values of the color ramp is different between the two events.

**Spatial and temporal characteristics of the two storms**

Hourly maximum (point) rainfall intensities of the two events were very similar with RI values well less than 1 year (Figure 3), suggesting that rain storms with similar hourly point intensities to the two events are frequent, occurring almost every year, in the study watershed. The 2-, 3- and 6-h maximum point rainfall intensities of the 6/28/2013 event were consistently higher than those of the 9/8/2011 event, with the RI value of 1.5, 3, and 8.5 years, respectively (Figure 3). The RI value of the 6/28/2013 event at the 12-h interval

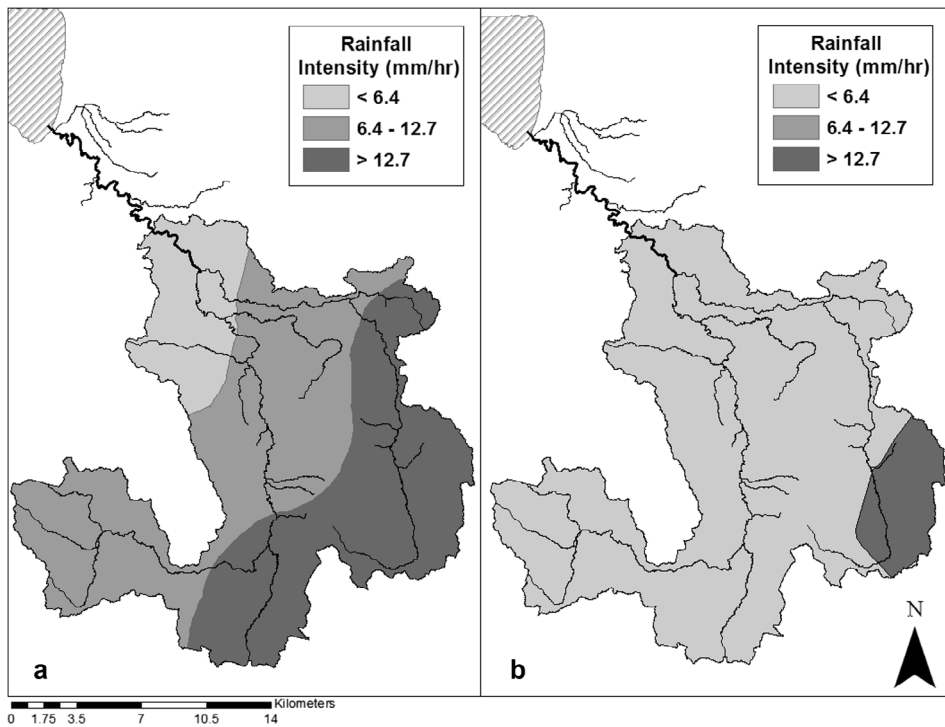


**Figure 5.** Examples of hourly rainfall distributions of the two selected events at (a) the 6th hour of the 6/28/2013 event and (b) the 2nd hour of the 9/8/2011 event.

**Table 1.** Areas covered by different rainfall intensities and their percentages in eight consecutive hours during the two selected events.

Hours	The 6/28/2013 event				The 9/8/2011 event			
	6.35 < RFI <sup>a</sup> < 12.7		RFI > 12.7		6.35 < RFI < 12.7		RFI > 12.7	
	Area	Percentage	Area	Percentage	Area	Percentage	Area	Percentage
1	14.16	4.5	0.00	0.0	1.74	0.6	0.00	0.0
2	61.52	19.5	36.8	11.7	288.6	91.5	26.9	8.5
3	6.31	2.0	0.00	0.0	163.8	51.9	0.00	0.0
4	21.03	6.7	18.4	5.8	0.35	0.1	0.00	0.0
5	44.48	14.1	44.4	14.1	58.8	18.6	0.00	0.0
6	135.6	43.0	80.6	25.6	208.9	66.2	0.00	0.0
7	147.6	46.8	121.9	38.7	314.8	99.8	0.64	0.2
8	179.7	57.0	19.5	6.2	307.9	97.6	7.51	2.4

<sup>a</sup>RFI: rainfall intensity (mm/h).

(i.e. the total event precipitation) was about 8 years, suggesting that the 6/28/2013 storm event was a normal heavy storm event. Nonetheless, the RI value of the 9/8/2011 event was about 21 years at the same interval and 42 years at the 24-h interval, much higher than that of the 6/28/2013 event. This signified that the total precipitation of the 9/8/2011 event was much greater than that of the 6/28/2013 event. The similarity and disparity between the two indicated that the 9/8/2011 storm lasted longer with a greater precipitation than the 6/28/2013 storm. Yet, it only generated a hydrological event with an 11-year peak discharge,

whereas the 8-year storm (6/28/2013) resulted in a flood with the peak discharge of 86 years. Therefore, the RI values of point rainfall intensities of the two storm events were apparently insufficient to explain those of the two peak discharges.

Severity diagrams deciphered the spatial variabilities of the two selected storm events. Within the 12-h duration of the 6/28/2013 event, rainfall initially had a RI less than 1 year for almost the entire watershed (dark blue color in Figure 4(a)). This was followed by an increase in the RI for the entire area until the time between the third and fourth hour, peaking around 4 years. From the fourth to the twelfth hour, the magnitude of rainfall increased quickly but focused on smaller and smaller areas (Figure 4(a)). The RI maximum, ranging between 7 and 11 years, occurred during this period, but only covered an area less than 60 km<sup>2</sup>. This spatial and temporal pattern indicated that high rainfall intensities of the 6/28/2013 storm were localized. The 9/8/2011 event displayed a different spatial and temporal pattern (Figure 4(b)). Initially, rainfall throughout the entire watershed had a 1-year RI. In the following 15 h, the magnitude of rainfall steadily increased over the entire area and reached that with a 26-year RI. The remaining eight hours were characterized by the continuous increase of the rainfall magnitude, with the rainfall extension gradually reducing to smaller areas.

The two severity diagrams show the distinct spatial patterns of the two events. The 6/28/2013 was relatively small by magnitude, but highly intense with localized foci. The 9/8/2011 event was high by magnitude (i.e. the RI value of the maximum point rainfall intensity), but less intense, with a prolonged period and an extensive distribution. Temporally, both events had a tendency of moving from upstream to downstream.

The proportion of the study area covered by rainfall intensity greater than 12.7 mm/h ranged from 5.8 to 38.7% for 5 consecutive hours within the 8-h period of the 6/28/2013 event (Figure 5(a), Table 1). For the 9/8/2011 event, however, this proportion only reached 8.5% for 1 h and 2.4% 5 h later (Figure 5(b), Table 1). These values confirmed the spatial pattern of the 6/26/2013 event illustrated by the severity diagram: it had localized high rainfall intensities. Within the same 8 h, the proportion of the study watershed covered by rainfall intensity between 6.35 and 12.7 mm/h was much higher for the 9/8/2011 event than in the 6/28/2013 event with the highest proportion (>60%) lasting four consecutive hours (Table 1). These values further corroborated the uniformly distributed pattern of the 9/8/2011 event with relatively high magnitudes displayed in its severity diagram. Thus, the different spatial patterns, rather than the magnitudes of the two storm events may be more important for generating the hydrological events of the associated magnitudes.

### **Rainfall-runoff dynamics of the two events**

The calculated rainfall coefficients showed that almost half of the precipitation (49%) was transferred into runoff during the 6/28/2013 event, while only 33% of it was turned into runoff during the 9/8/2011 event. This difference may be explained by the results of watershed modeling. DWSM simulation showed that for the 6/28/2013 event,  $Q_{\text{peak}}$  was about 6.6% higher than the measured one and lagged only by 15 min (Figure 6(a)). The value of  $V$  was about 15% less than the measured value. For the 9/8/2011 event, the predicted  $Q_{\text{peak}}$  and  $V$  were 2.3 and 2.2% higher than the measured with  $Q_{\text{peak}}$  about 15 min lagged behind the measured one (Figure 6(b)). These results indicated that DWSM effectively captured rainfall-runoff dynamics of the two events.

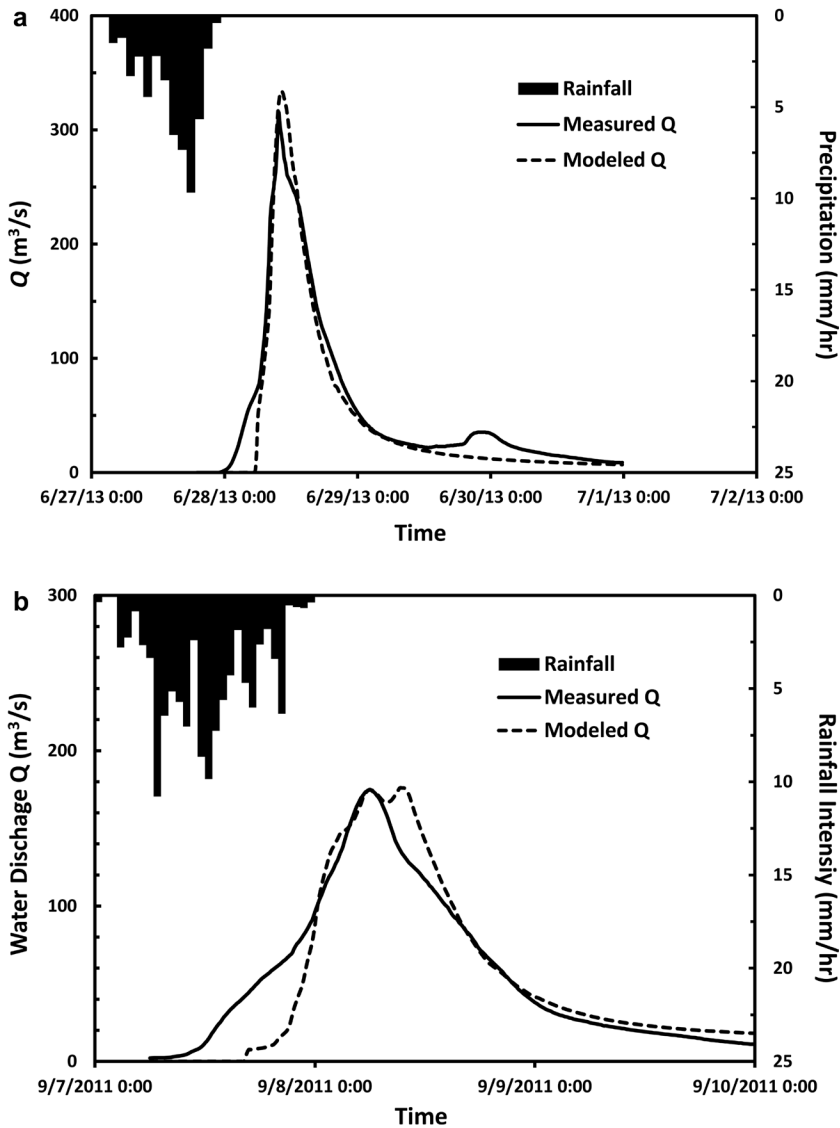


**Figure 6.** Comparison of the measured with predicted hydrographs using DWSM for the two selected events. (a) The 6/28/2013 event and (b) the 9/8/2011 event.

**Table 2.** Values of the six adjustable parameters for the two simulated events.

	The 6/28/2013 event	The 9/8/2011 event
CNAF	1.30	0.75
$a$	0.2	0.05
FAFO	4.1	4.5
FAFC	1.1	0.5
COND	0.34	0.5
CONT	3.26	60

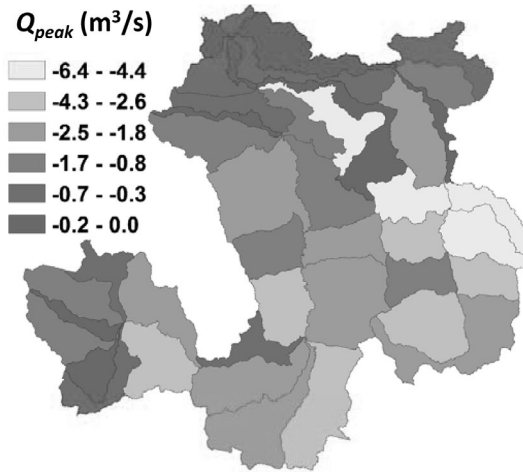


**Figure 7.** Spatial variations of peak discharges predicted using DWSM for the two selected events.

Values of CNAF for the 6/28/2013 event was much higher than that of the 9/8/2011 event, while that of  $a$  for the first event was clearly higher than that for the second event (Table 2). The higher CNAF value suggested that more stream flow was generated during the 6/28/2013 event, which was consistent with its higher rainfall coefficient. The higher  $a$  value suggested that ASM tended to be higher in the 6/28/2013 event than in the 9/8/2011 event. Similar FAFO values in the two events and the higher FAFC value in the 6/28/2013 event indicated that the overall surface friction on overland elements was comparable in two events, whereas the general resistance to flow in channels was slightly greater in the 6/28/2013 event than in the 9/8/2011 event (Table 2), perhaps because of higher suspended sediment concentrations carried during the 6/28/2013 event. COND was marginally higher in the 9/8/2011 event than in the 6/28/2013 event, while CONT was much lower in the 6/28/2013 event than during the 9/8/2011 event. Because CONT has much less effect on the predicted runoff than COND has, these values suggested that the amount of subsurface flow was similar in the two events.

Values of these parameters highlight the different rainfall-runoff responses of the two hydrological events. The 6/28/2013 event was dominated by the infiltration excess process, which caused higher magnitude, but shorter period flow rates. By contrast, the 9/8/2011 event was controlled by both the infiltration and saturation excess processes, which led to lower magnitude, but longer period flow rates. This difference was further supported by the generally higher  $Q_{\text{peak}}$  values of the 6/28/2013 event in all 42 overland elements than those of the 9/8/2011 event (Figure 7). In theory, the higher ASM in the 6/28/2013 event may also contribute to the higher magnitude of  $Q_{\text{peak}}$  of the 6/28/2013 event, which was also true in other areas of New York State (Jessup & DeGaetano, 2008). Since the predicted hydrograph is less affected by the change of ASM than the change of CNAF (Gao et al., 2015), the higher  $Q_{\text{peak}}$  values for the 6/28/2013 event was primarily attributed to the higher CNAF value of this event (Table 2). Therefore, the high magnitude of the 6/28/2013 hydrological event resulted from the higher efficiency of rainfall-runoff transformation dominated by the infiltration excess process.

## Discussion

Extreme rainfall is a typical cause for hazardous flood discharges in rivers under various climatic zones (Downs, Dusterhoff, & Sears, 2013; Filizola et al., 2014; Jena et al., 2014; Parajka et al., 2010) and deserves more attention. Here, we demonstrated that the 6/28/2013 storm was a typically heavy rainfall event that resulted in a catastrophic hydrological event in the study watershed. This event had a unique “upgrade”-magnitude conversion pattern – that is, a storm with a RI of 8 years generated a hydrological event with the  $Q_{\text{peak}}$  having a RI of 86 years. Another extreme flood in 1922 within the same area appeared to have the same pattern because it lasted “over one night,” though no climatic and hydrological data were available at that time (ABDCE, 1973). Our analyses indicated that the upgrade-magnitude pattern of the 6/28/2013 event was the result of two combined factors. First, spatially localized high rainfall intensities facilitated the supply of a relatively high amount of precipitation within a short time period (less than 8 h), though the magnitude of the total precipitation was not very high. Second, the typical physiographic settings of the watershed (e.g. land use/cover, soil types, topographic patterns, and drainage density) assured the dominance of the infiltration excess process, which promoted the high efficiency of the rainfall-runoff transformation and created the historical flooding event.

The 6/28/2013 event was not caused by the extreme rainfall (Smith, Baeck, Villarini, & Krajewski, 2010), which typically leads to a “downgrade”-magnitude conversion pattern, similar to the 9/8/2011 event (i.e. the two RI values for the storm and the associated  $Q_{\text{peak}}$  value were 42 and 11 years, respectively). From the perspective of rainfall-runoff transformation, the “upgrade”-magnitude nature of the 6/28/2013 event suggested that a watershed may not always serve as a “filter” to generate the peak discharge with reduced magnitude compared with that of the rainfall event. For a given watershed, whether a storm would cause an “upgrade”-magnitude or “downgrade”-magnitude flood event seems more dependent on the spatial and temporal pattern of the rainfall event, rather than the magnitude of the total precipitation. This is a new perspective of emphasizing the importance of spatial distribution of a rainfall event.

The “upgrade”-magnitude pattern of the 6/28/2013 event posed an additional challenge to the threshold-based flash flood warning method (Norbiato, Borga, Degli Esposti, Gaume, & Anquetin, 2008; Ntelekos, Georgakakos, & Krajewski, 2006) because an extreme flood may be caused by an under-threshold storm event. Moreover, the risk from floods similar to the 6/28/2013 event to the local communities may be even higher than those caused by extreme storm events because these floods tend to be “surprising” since they are induced by regular heavy rainfall events such that individuals and local agencies are less prepared for them (Botzen, Aerts, & van den Bergh, 2009).

## Conclusions

Flood damages caused by an extreme hydrological event (i.e. the 6/28/2013 event) with a RI of 86 years in Central New York were extensive and severe. Yet, this flood was produced by a frequently intense rainstorm whose RI value for the total precipitation was only about 8 years. This event was unique compared with the 9/8/2011 event that had RI values of 42 and 11 years, respectively. The “upgrade”-magnitude conversion pattern of the 6/28/2013 event was caused by spatially localized high rainfall intensities and the efficient

rainfall-runoff transformation through the infiltration excess process. The first was confirmed by the developed severity diagram and the subsequent quantification of the spatial and temporal pattern of this event. The second was evidenced in watershed modeling using a physically based model, DWSM.

The causes of this extreme flood highlighted two findings of this study. First, characterizing spatial structure of a storm event is more important than calculating the total amount of precipitation for improving flood forecasts. Second, the surface area of a watershed may encourage the rainfall-runoff transformation, though it typically serves as a filter to reduce the magnitude of the rainfall event.

Theoretically, this kind of extreme flood event is more difficult to predict because it is caused by locally intensified rainfall intensities rather than the magnitude of the total precipitation. Practically, it is more harmful in that it was triggered by a “normal” storm such that local residents may be less prepared for the potential flood damages. Therefore, this type of extreme event requires more attention.

## Acknowledgement

We thank Scoot Ingmire, the director of the Madison County Planning Department and Jon Rauscher, the leading engineer in the Department of Engineering & Public Works, City of Oneida for providing us the information about physical damages and economic losses within the city caused by the 6/28/2013 extreme event.

## Disclosure statement

No potential conflict of interest was reported by the authors.

## References

- ABDCE. (1973). *Flood plain information: Oneida Creek*. New York, NY: Buffalo.
- Andres-Domenech, I., Garcia-Bartual, R., Montanari, A., & Marco, J. B. (2015). Climate and hydrological variability: The catchment filtering role. *Hydrology and Earth System Sciences*, 19, 379–387. doi:10.5194/hess-19-379-2015
- Apurv, T., Mehrotra, R., Sharma, A., Goyal, M. K., & Dutta, S. (2015). Impact of climate change on floods in the Brahmaputra basin using CMIP5 decadal predictions. *Journal of Hydrology*, 527, 281–291. doi:10.1016/j.jhydrol.2015.04.056
- Arghius, V., Ozunu, A., Samara, I., & Rosian, G. (2014). Results of the post flash-flood disaster investigations in the Transylvanian Depression (Romania) during the last decade (2001–2010). *Natural Hazards and Earth System Science*, 14, 535–544.
- Arnauda, P., Bouvier, C., Cisneros, L., & Dominguez, R. (2002). Influence of rainfall spatial variability on flood prediction. *Journal of Hydrology*, 260, 216–230.
- Bargaoui, Z. K., & Bardossy, A. (2015). Modeling short duration extreme precipitation patterns using copula and generalized maximum pseudo-likelihood estimation with censoring. *Advances in Water Resources*, 84, 1–13. doi:10.1016/j.advwatres.2015.07.006
- Bedient, P. B., & Huber, W. C. (2002). *Hydrology and floodplain analysis*. Upper Saddle River, NJ: Prentice Hall.
- Beven, K. J. (2001). *Rainfall-runoff modeling: The primer*. Chichester: Wiley.
- Billi, P., Alemu, Y. T., & Ciampalini, R. (2015). Increased frequency of flash floods in Dire Dawa, Ethiopia: Change in rainfall intensity or human impact? *Natural Hazards*, 76, 1373–1394. doi:10.1007/s11069-014-1554-0

- Borah, D. K. (2011). Hydrologic procedures of storm event watershed models: A comprehensive review and comparison. *Hydrological Processes*, 25, 3472–3489.
- Borah, D. K., Bera, M., & Xia, R. (2004). Storm event flow and sediment simulations in agricultural watersheds using DWSM. *Transactions of the ASAE*, 47, 1539–1559.
- Borah, D. K., Xia, R., & Bera, M. (2002). DWSM – A dynamic watershed simulation model. In V. P. Singh & D. Frevert (Eds.), *Mathematical models of small watershed hydrology and applications* (pp. 113–166). Highlands Ranch, CO: Water Resources Publications LLC.
- Borga, M., Anagnostou, E. N., Bloschl, G., & Creutin, J.-D. (2011). Flash flood forecasting, warning and risk management: The HYDRATE project. *Environmental Science & Policy*, 14, 834–844.
- Botzen, W. J. W., Aerts, J. C. J. H., & van den Bergh, J. C. J. M. (2009). Dependence of flood risk perceptions on socioeconomic and objective risk factors. *Water Resources Research*, 45, W10440. doi:10.11029/12009WR007743
- Carvalho, R. C., & Woodroffe, C. D. (2015). Rainfall variability in the Shoalhaven River catchment and its relation to climatic indices. *Water Resources Management*, 29, 4963–4976. doi:10.1007/s11269-015-1098-4
- Ceresetti, D., Anquetin, S., Molinié, G., Leblois, E., & Creutin, J.-D. (2011). Multiscale evaluation of extreme rainfall event predictions using severity diagrams. *Weather and Forecasting*, 27, 174–188. doi:110.1175/WAF-D-1111-00003.00001
- Chow, V. T., Maidment, D. R., & Mays, L. W. (1988). *Applied hydrology*. New York, NY: McGraw-Hill Book Company.
- CNYRPDB. (2003). *Oneida Lake state of lake and watershed report*. New York, NY: Syracuse.
- Cross, J. A. (2014). Disaster devastation of US communities: Long-term demographic consequences. *Environmental Hazards*, 13, 73–91.
- Death, R. G., Fuller, I. C., & Macklin, M. G. (2015). Resetting the river template: The potential for climate-related extreme floods to transform river geomorphology and ecology. *Freshwater Biology*, 60, 2477–2496. doi:10.1111/fwb.12639
- Downs, P. W., Dusterhoff, S. R., & Sears, W. A. (2013). Reach-scale channel sensitivity to multiple human activities and natural events: Lower Santa Clara River, California, USA. *Geomorphology*, 189, 121–134.
- Faures, J. M., Goodrich, D. C., Woolhiser, D. A., & Sorooshian, S. (1995). Impact of small-scale spatial rainfall variability on runoff modeling. *Journal of Hydrology*, 173, 309–326.
- Filizola, N., Latrubesse, E. M., Fraizy, P., Souza, R., Guimarães, V., & Guyot, J.-L. (2014). Was the 2009 flood the most hazardous or the largest ever recorded in the Amazon? *Geomorphology*, 215, 99–105.
- Foulds, S. A., Griffiths, H. M., Macklin, M. G., & Brewer, P. A. (2014). Geomorphological records of extreme floods and their relationship to decadal-scale climate change. *Geomorphology*, 216, 193–207.
- Fuller, I. C. (2007). Geomorphic work during a “150-year” storm: Contrasting behaviors of river channels in a New Zealand catchment. *Annals of the Association of American Geographers*, 97, 665–676.
- Gamoyo, M., Reason, C., & Obura, D. (2015). Rainfall variability over the East African coast. *Theoretical and Applied Climatology*, 120, 311–322. doi:10.1007/s00704-014-1171-6
- Gao, P., Borah, D., & Yi, C. (2015). Storm Event Flow and Sediment Simulations in a Central New York Watershed: Model Testing and Parameter Analyses. *Transactions of the American Society of Agricultural and Biological Engineers*, 85(5), 1241–1252.
- Gao, P., Borah, D. K., & Josefson, M. (2013). Evaluation of the storm event model DWSM on a medium-sized watershed in central New York, USA. *Journal of Urban and Environmental Engineering*, 7(1), 1–7.
- Gao, P., & Josefson, M. (2012a). Event-based suspended sediment dynamics in a central New York watershed. *Geomorphology*, 139–140, 425–437. doi:10.1016/j.geomorph.2011.11.007
- Gao, P., & Josefson, M. (2012b). Temporal variations of suspended sediment transport in Oneida Creek watershed, Central New York. *Journal of Hydrology*, 426–427, 17–27.
- Gao, P., & Puckett, J. (2012). A new approach for linking event-based upland sediment sources to downstream suspended sediment transport. *Earth Surface Processes and Landforms*, 37, 169–179. doi:10.1002/esp.2229

- Gonzalez, A., Temimi, M., & Khanbilvardi, R. (2015). Adjustment to the curve number (NRCS-CN) to account for the vegetation effect on hydrological processes. *Hydrological Sciences Journal*, 60, 591–605. doi:10.1080/02626667.2014.898119
- Guo, W. J., Wang, C. H., Zeng, X. M., Ma, T. F., & Yang, H. (2015). Quantifying the spatial variability of rainfall and flow routing on flood response across scales. *Environmental Earth Sciences*, 74, 6421–6430. doi:10.1007/s12665-015-4456-x
- Han, L., Xu, Y., Pan, G., Deng, X., Hu, C., Xu, H., & Shi, H. (2015). Changing properties of precipitation extremes in the urban areas, Yangtze River Delta, China, during 1957–2013. *Natural Hazards*, 79, 437–454. doi:10.1007/s11069-015-1850-3
- Hawkins, R. H., Ward, T. J., Woodward, D. E., & Van Mullem, J. A. (2008). *Curve number hydrology*. Reston, VA: American Society of Civil Engineers: Environmental and Water Resources Institute (EWRI).
- He, H. M., Zhou, J., Yu, Q., Tian, Y. Q., & Chen, R. F. (2007). Flood frequency and routing processes at a confluence of the middle Yellow River in China. *River Research and Applications*, 23, 407–427.
- Huntington, T. G. (2006). Evidence for intensification of the global water cycle: Review and synthesis. *Journal of Hydrology*, 319, 83–95.
- IPCC. (2013). *Climate change 2013: The physical science basis contribution of Working Group I to the Fifth Assessment Report of the Intergovernmental Panel on Climate Change*. (T. F. Stocker, D. Qin, G.-K. Plattner, M. Tignor, S. K. Allen, A. Boschung, ... P. M. Midgley Eds.). Cambridge: Cambridge University Press. doi:10.1017/CBO9781107415324
- Jena, P. P., Chatterjee, C., Pradhan, G., & Mishra, A. (2014). Are recent frequent high floods in Mahanadi basin in eastern India due to increase in extreme rainfalls? *Journal of Hydrology*, 517, 847–862.
- Jessup, S. M., & DeGaetano, A. T. (2008). A statistical comparison of the properties of flash flooding and nonflooding precipitation events in portions of New York and Pennsylvania. *Weather and Forecasting*, 23, 114–130. doi:10.1175/2007WAF2006066.2006061
- Kundzewicz, Z. W., Kanae, S., Seneviratne, S. I., Handmer, J., Nicholls, N., Peduzzi, P., ... Sherstyukov, B. (2013). Large floods in Europe, 1985–2009. *Hydrological Sciences Journal*, 58(1), 1–7.
- Mallakpour, I., & Villarini, G. (2015). The changing nature of flooding across the central United States. *Nature Climate Change*, 5, 250–254. doi:10.1038/nclimate2516
- Marchi, L., Borga, M., Preciso, E., Sangati, M., Gaume, E., Bain, V., ... Pogaènik, N. (2009). Comprehensive post-event survey of a flash flood in Western Slovenia: Observation strategy and lessons learned. *Hydrological Processes*, 23, 3761–3770.
- Matthews, T., Murphy, C., Wilby, R. L., & Harrigan, S. (2014). Stormiest winter on record for Ireland and UK. *Nature Climate Change*, 4, 738–740.
- McCuen, R. (2004). *Hydrologic analysis and design*. Upper Saddle River, NJ: Pearson Prentice Hall.
- Méndez-Lázaro, P. A., Nieves-Santiago, A., & Miranda-Bermúdez, J. (2014). Trends in total rainfall, heavy rain events, and number of dry days in San Juan, Puerto Rico, 1955–2009. *Ecology and Society*, 19, 50.
- Mendizabal, M., Sepúlveda, J., & Torp, P. (2014). Climate change impacts on flood events and its consequences on human in Deba River. *International Journal of Environmental Research*, 8, 221–230.
- Mirus, B. B., Ebel, B. A., Heppner, C. S., & Loague, K. (2011). Assessing the detail needed to capture rainfall-runoff dynamics with physics-based hydrologic response simulation. *Water Resources Research*, 47, W00H10. doi:10.1029/2010WR009906
- Norbiato, D., Borga, M., Degli Esposti, S., Gaume, E., & Anquetin, S. (2008). Flash flood warning based on rainfall thresholds and soil moisture conditions: An assessment for gauged and ungauged basins. *Journal of Hydrology*, 362, 274–290. doi:10.1016/j.jhydrol.2008.1008.1023
- Ntelekos, A. A., Georgakakos, K. P., & Krajewski, W. F. (2006). On the uncertainties of flash flood guidance: Toward probabilistic forecasting of flash floods. *Journal of Hydrometeorology*, 7, 896–915. doi:10.1175/JHM1529.1171
- Paixao, E., Mirza, M. M. Q., Shephard, M. W., Auld, H., Klaassen, J., & Smith, G. (2015). An integrated approach for identifying homogeneous regions of extreme rainfall events and estimating IDF curves in Southern Ontario, Canada: Incorporating radar observations. *Journal of Hydrology*, 528, 734–750. doi:10.1016/j.jhydrol.2015.06.015

- Panthi, J., Dahal, P., Shrestha, M. L., Aryal, S., Krakauer, N. Y., Pradhanang, S. M., ... Karki, R. (2015). Spatial and temporal variability of rainfall in the Gandaki River basin of Nepal Himalaya. *Climate*, 3, 210–226. doi:10.3390/cli3010210
- Parajka, J., Kohnova', S., Ba'lint, G., Barbuc, M., Borga, M., Claps, P., ... Blo' schl, G. (2010). Seasonal characteristics of flood regimes across the Alpine-Carpathian range. *Journal of Hydrology*, 394, 78–89. doi:10.1016/j.jhydrol.2010.1005.1015
- Ramos, M. H., Creutin, J.-D., & Leblois, E. (2005). Visualization of storm severity. *Journal of Hydrology*, 315, 295–307.
- Saulnier, G.-M., & Le Lay, M. (2009). Sensitivity of flash-flood simulations on the volume, the intensity, and the localization of rainfall in the Cévennes-Vivarais region (France). *Water Resources Research*, 45, W10425. doi:10.4101.11029/12008WR006906
- Schiermeier, Q. (2011). Increased flood risk linked to global warming. *Nature*, 470, 316.
- Schuurmans, J. M., & Bierkens, M. F. P. (2007). Effect of spatial distribution of daily rainfall on interior catchment response of a distributed hydrological model. *Hydrology and Earth System Sciences*, 11, 677–693.
- Simoes, N. E., Ochoa-Rodriguez, S., Wang, L.-P., Pina, R. D., Marques, A. S., Onof, C., & Leitao, J. P. (2015). Stochastic urban pluvial flood hazard maps based upon a spatial-temporal rainfall generator. *Water*, 7, 3396–3406. doi:10.3390/w7073396
- Smith, J. A., Baeck, M. L., Villarini, G., & Krajewski, W. F. (2010). The hydrology and hydrometeorology of flooding in the Delaware River basin. *Journal of Hydrometeorology*, 11, 841–859.
- Soulis, K. X., & Valiantzas, J. D. (2012). SCS-CN parameter determination using rainfall-runoff data in heterogeneous watersheds – The two-CN system approach. *Hydrology and Earth System Sciences*, 16, 1001–1015. doi:10.5194/hess-1016-1001-2012
- Stevenson, S. N., & Schumacher, R. S. (2014). A 10-Year survey of extreme rainfall events in the Central and Eastern United States using gridded multisensor precipitation analyses. *Monthly Weather Review*, 142, 3147–3162.
- Vié, B., Molinié, G., Nuissier, O., Vincendon, B., Ducrocq, V., Bouttier, F., & Richard, E. (2012). Hydro-meteorological evaluation of a convection-permitting ensemble prediction system for Mediterranean heavy precipitating events. *Natural Hazards and Earth System Science*, 12, 2631–2645. doi: 2610.5194/nhess-2612-2631-2012
- Vincendon, B., Ducrocq, V., Nuissier, O., & Vié, B. (2011). Perturbation of convection-permitting NWP forecasts for flash-flood ensemble forecasting. *Natural Hazards and Earth System Science*, 11, 1529–1544. doi: 2610.5194/nhess-2612-2631-2012
- Yin, H. F., & Li, C. G. (2001). Human impact on floods and flood disasters on the Yangtze River. *Geomorphology*, 41, 105–109.
- Yu, F. L., Chen, Z. Y., Ren, X. Y., & Yang, G. F. (2009). Analysis of historical floods on the Yangtze River, China: Characteristics and explanations. *Geomorphology*, 113, 209–216.
- Zhang, Y. Z., Huang, C. C., Pang, J. L., Zha, X. C., Zhou, Y. L., & Gu, H. L. (2013). Holocene paleofloods related to climatic events in the upper reaches of the Hanjiang River valley, middle Yangtze River basin, China. *Geomorphology*, 195, 1–12.